



## Electrochemical etching of AlGaN for the realization of thin-film devices

Downloaded from: <https://research.chalmers.se>, 2025-12-04 22:48 UTC

Citation for the original published paper (version of record):




Bergmann, M., Enslin, J., Yapparov, R. et al (2019). Electrochemical etching of AlGaN for the realization of thin-film devices. Applied Physics Letters, 115(18): 182103-.  
<http://dx.doi.org/10.1063/1.5120397>

N.B. When citing this work, cite the original published paper.

# Electrochemical etching of AlGa<sub>N</sub> for the realization of thin-film devices F

Cite as: Appl. Phys. Lett. **115**, 182103 (2019); <https://doi.org/10.1063/1.5120397>

Submitted: 17 July 2019 . Accepted: 15 October 2019 . Published Online: 30 October 2019

Michael A. Bergmann, Johannes Enslin, Rinat Yapparov , Filip Hjort , Björn Wickman, Saulius Marcinkevičius, Tim Wernicke, Michael Kneissl, and Åsa Haglund 

## COLLECTIONS

F This paper was selected as Featured



View Online



Export Citation



CrossMark

## ARTICLES YOU MAY BE INTERESTED IN

**12 GHz spontaneous optical bandwidth tunnel junction light-emitting transistor**

Applied Physics Letters **115**, 181102 (2019); <https://doi.org/10.1063/1.5124959>

**Effect of hydrogen derived from oxygen source on low-temperature ferroelectric TiN/Hf<sub>0.5</sub>Zr<sub>0.5</sub>O<sub>2</sub>/TiN capacitors**

Applied Physics Letters **115**, 182901 (2019); <https://doi.org/10.1063/1.5126144>

**High power surface emitting InGa<sub>N</sub> superluminescent light-emitting diodes**

Applied Physics Letters **115**, 171102 (2019); <https://doi.org/10.1063/1.5118953>



**Measure Ready**  
**M91 FastHall™ Controller**

A revolutionary new instrument  
for complete Hall analysis

See the video 



# Electrochemical etching of AlGa<sub>N</sub> for the realization of thin-film devices

Cite as: Appl. Phys. Lett. **115**, 182103 (2019); doi: [10.1063/1.5120397](https://doi.org/10.1063/1.5120397)

Submitted: 17 July 2019 · Accepted: 15 October 2019 ·

Published Online: 30 October 2019



View Online



Export Citation



CrossMark

Michael A. Bergmann,<sup>1,a)</sup> Johannes Enslin,<sup>2</sup> Rinat Yapparov,<sup>3</sup>  Filip Hjort,<sup>1</sup>  Björn Wickman,<sup>4</sup> Saulius Marcinkevičius,<sup>3</sup> Tim Wernicke,<sup>2</sup> Michael Kneissl,<sup>2</sup> and Åsa Haglund<sup>1</sup> 

## AFFILIATIONS

<sup>1</sup>Department of Microtechnology and Nanoscience, Chalmers University of Technology, 41296 Gothenburg, Sweden

<sup>2</sup>Institute of Solid State Physics, Technische Universität Berlin, 10623 Berlin, Germany

<sup>3</sup>Department of Applied Physics, KTH Royal Institute of Technology, 16440 Kista, Sweden

<sup>4</sup>Department of Physics, Chalmers University of Technology, 41296 Gothenburg, Sweden

a)michael.bergmann@chalmers.se

## ABSTRACT

Heterogeneously integrated AlGa<sub>N</sub> epitaxial layers will be essential for future optical and electrical devices like thin-film flip-chip ultraviolet (UV) light-emitting diodes, UV vertical-cavity surface-emitting lasers, and high-electron mobility transistors on efficient heat sinks. Such AlGa<sub>N</sub>-membranes will also enable flexible and micromechanical devices. However, to develop a method to separate the AlGa<sub>N</sub>-device membranes from the substrate has proven to be challenging, in particular, for high-quality device materials, which require the use of a lattice-matched AlGa<sub>N</sub> sacrificial layer. We demonstrate an electrochemical etching method by which it is possible to achieve complete lateral etching of an AlGa<sub>N</sub> sacrificial layer with up to 50% Al-content. The influence of etching voltage and the Al-content of the sacrificial layer on the etching process is investigated. The etched N-polar surface shows the same macroscopic topography as that of the as-grown epitaxial structure, and the root-mean square roughness is 3.5 nm for 1 μm × 1 μm scan areas. Separated device layers have a well-defined thickness and smooth etched surfaces. Transferred multi-quantum-well structures were fabricated and investigated by time-resolved photoluminescence measurements. The quantum wells showed no sign of degradation caused by the thin-film process.

© 2019 Author(s). All article content, except where otherwise noted, is licensed under a Creative Commons Attribution (CC BY) license (<http://creativecommons.org/licenses/by/4.0/>). <https://doi.org/10.1063/1.5120397>

AlGa<sub>N</sub> is used in a variety of devices for different applications such as ultraviolet C (UVC) light-emitting diodes (LEDs) for water purification<sup>1</sup> and high-electron mobility transistors (HEMTs) for high power applications.<sup>2</sup> By separating the device layers from their substrates, the device performance can be improved and more advanced device concepts can be realized such as thin-film flip-chip LEDs, vertical-cavity surface-emitting lasers (VCSELs) with double dielectric distributed Bragg reflectors, high-quality microring resonators, photonic crystal resonators, and HEMTs on efficient heat sinks or flexible substrates. However, achieving lift-off of AlGa<sub>N</sub> device layers from the substrate has proven to be challenging.

Until now, most substrate removal attempts for AlGa<sub>N</sub>-based optical devices have focused on laser induced lift-off. AlGa<sub>N</sub>-based thin-film ultraviolet (UV) LEDs have been fabricated by either laser lift-off of GaN<sup>3</sup> or AlGa<sub>N</sub><sup>4</sup> to remove the substrate. Thermal decomposition of GaN is an established process, but a GaN sacrificial layer does not allow for the growth of AlGa<sub>N</sub> device layers on top with a

high crystalline quality due to the lattice mismatch, leading to cracking of the AlGa<sub>N</sub> layer<sup>5</sup> and thus strongly limiting the aluminum content and layer thickness. Using a sacrificial layer of AlGa<sub>N</sub> instead would ensure a high crystalline quality of the device layers. However, the decomposition of AlGa<sub>N</sub> yields rigid aluminum residues that are difficult to remove.<sup>4</sup> In addition, strained epitaxial layers have a tendency to crack when exposed to elevated temperatures during laser irradiation.<sup>4</sup> Additionally, laser lift-off creates rough surfaces and it is not possible to accurately control the thickness. Therefore, it is not an optimal method for optical devices such as VCSELs and microring resonators that require low scattering losses and precise control of modal properties, i.e., the membrane thickness.

A promising method to achieve GaN and AlGa<sub>N</sub> membranes with a low surface roughness and epitaxially defined thickness is doping-selective electrochemical etching of sacrificial GaN layers.<sup>6</sup> This technique has been used to realize various thin-film devices like AlGa<sub>N</sub>-based HEMTs,<sup>7</sup> AlGa<sub>N</sub>-based microring resonators,<sup>8</sup> and

piezoelectric energy harvesters.<sup>9</sup> Depending on the doping concentration in the GaN sacrificial layer and the applied voltage during the electrochemical etching, the sacrificial layer can either be completely etched or porosified.<sup>10</sup> To enable AlGaIn-based devices with a high crystalline quality and high aluminum content, the sacrificial layer should be of AlGaIn rather than GaN to avoid strain relaxation and formation of threading dislocations. There are so far only a few reports on porosification of AlGaIn by electrochemical etching.<sup>11–14</sup> In this work, we demonstrate electrochemical etching of AlGaIn with an Al content of up to 50% and investigate the dependence of the morphology of the sacrificial layer after the etching on the applied etching voltage and the Al-composition. Furthermore, we show the usability of this method for the realization of thin-film devices by the transfer of a multi-quantum-well (MQW) containing structure and the optical characterization of the transferred device layers.

The epitaxial layers were grown on a relaxed n-doped  $\text{Al}_{0.5}\text{Ga}_{0.5}\text{N}:\text{Si}$  pseudosubstrate with a doping level of  $[\text{Si}] = 2 \times 10^{18} \text{ cm}^{-3}$  on top of a c-plane AlN/sapphire substrate by metal organic vapor phase epitaxy in a close coupled showerhead reactor.<sup>15</sup> This n-doped template ensures a uniform electrochemical etching across the sample by spreading the current. On top of the template, a 225 nm  $\text{n-Al}_{0.5}\text{Ga}_{0.5}\text{N}$  etch stop layer with a reduced doping of  $[\text{Si}] = 0.5 \times 10^{18} \text{ cm}^{-3}$  was grown to prevent etching of the doped template. The next layer is a 130 nm  $\text{n-Al}_x\text{Ga}_{1-x}\text{N}$  layer, which serves as the sacrificial layer with a doping level of  $[\text{Si}] = 2 \times 10^{19} \text{ cm}^{-3}$  and an Al-composition  $x = [11\%, 27\%, 39\%, 50\%]$  for four different samples. The doping level was the same in all samples and was chosen to be as high as possible while still ensuring a high layer quality, to achieve a large etch selectivity between the sacrificial layer and the etch stop layers.<sup>6</sup> The last layer on top of the sacrificial layer is an unintentionally doped  $\text{Al}_{0.5}\text{Ga}_{0.5}\text{N}$  layer with a thickness of 580 nm for the samples with an Al-composition of  $x = [27\%, 39\%, 50\%]$  in the sacrificial layer and 1900 nm for the samples with an Al-composition of  $x = 11\%$  in the sacrificial layer. High resolution X-ray diffraction investigations of the grown samples show pseudomorphically grown sacrificial layers and  $\text{Al}_{0.5}\text{Ga}_{0.5}\text{N}:\text{Si}$  layers on top of the pseudosubstrate for all sacrificial layer compositions.

Figure 1(a) shows the sample design that was used for the electrochemical etching series. The sample fabrication started with dry etching of via holes with a diameter of  $10 \mu\text{m}$  in a  $7 \times 9$  array with a pitch of  $400 \mu\text{m}$  using chlorine-based inductively coupled plasma reactive-ion etching (ICP-RIE) into the current spreading layer to fully expose the sacrificial layer. To apply a bias voltage to the sample during the electrochemical etching, a V/Al/V/Au (15/80/20/95 nm) contact to the  $\text{n-AlGaIn}$  current spreading layer was formed using e-beam evaporation and lift-off. The n-contact was annealed at  $700^\circ\text{C}$  in a  $\text{N}_2$  atmosphere to reduce the contact resistance. In the last step, the top surface of the formed mesa structure was protected with a  $1.3\text{-}\mu\text{m}$  thick S1813 photoresist. Electrochemical etching was performed using a BioLogic SP-300 potentiostat in a three-electrode setup as illustrated in Fig. 1(b). The electrolyte, 0.3 M nitric acid, was constantly stirred during the etching process using a magnetic stir bar. A constant positive potential was applied to the AlGaIn sample, which served as the working electrode (WE) relative to a Ag/AgCl reference electrode (RE) and a graphite rod that was used as the counter electrode (CE) to regulate the current flow. The applied etching voltages were +15 V, +20 V, +25 V, and +30 V relative to the Ag/AgCl reference electrode. During

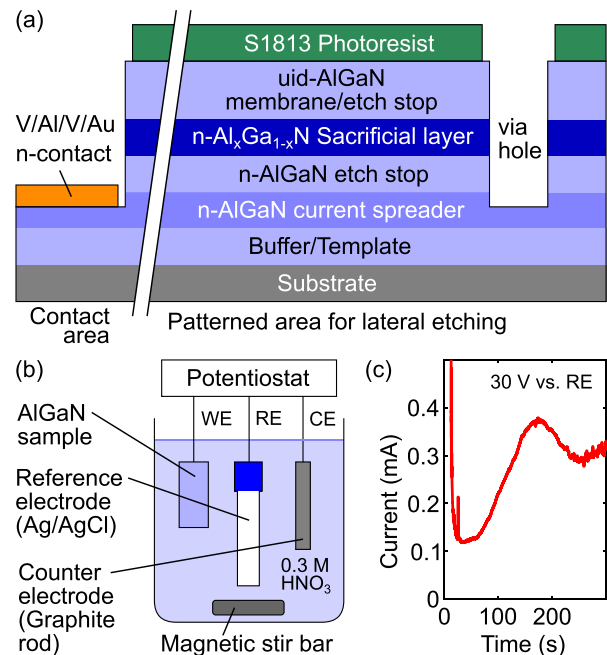


FIG. 1. Schematic of (a) the AlGaIn sample structure, (b) the three-electrode setup used for the electrochemical etching, and (c) etching current vs time for etching an  $\text{Al}_{0.11}\text{Ga}_{0.89}\text{N}$  sacrificial layer at 30 V.

the etching, no intentional heating or illumination was used. The exposed part of the sample was the via array and the edge of the  $5 \text{ mm} \times 10 \text{ mm}$  sample. Etching currents were in the low milliamper range [see Fig. 1(c)] and showed a similar trend to that reported in previous works.<sup>16</sup> After the etching process, the samples were rinsed with de-ionized water and left to dry in air.

Figure 2 shows an optical microscopy image of a sample with a sacrificial layer containing 11% Al after electrochemical etching for two and five minutes at 30 V vs Ag/AgCl ref. In Fig. 2(a), the bright circular areas depict the parts where the sacrificial layer is etched. As seen, the lateral etching that is initiated in the via holes proceeds isotropically. Therefore, the etch front area increases, and with that, also the current increases [compare Fig. 1(c)].<sup>16</sup> However, the etching current also contains contributions from etching at the sample edge.

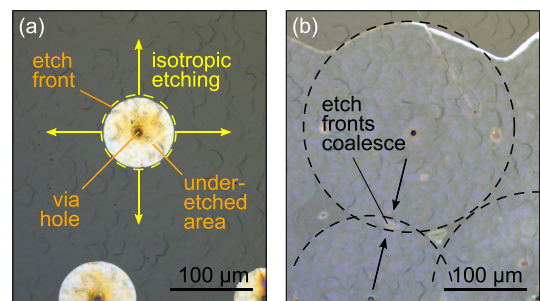
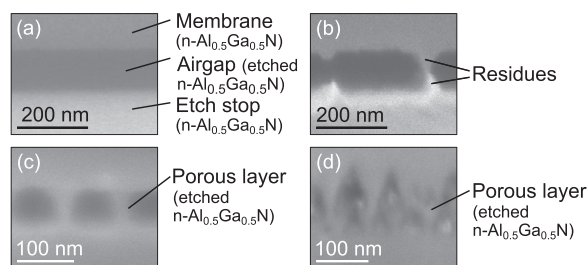


FIG. 2. Top view optical microscopy image of the sample with an  $\text{Al}_{0.11}\text{Ga}_{0.89}\text{N}$  sacrificial layer after electrochemical etching at 30 V for (a) 2 min and (b) 5 min.

Eventually, the etch fronts merge and a continuous air gap is formed [see Fig. 2(b)].

The morphology of the sacrificial layer after electrochemical etching was studied in the cross-sectional view by scanning electron microscopy (SEM). Figure 3 shows the cross section of four samples, all having the same sacrificial layer with an Al content of 50%, but etched at different voltages. Only the sacrificial layer was etched, whereas the etch stop layers on top and bottom are not affected, i.e., not porosified. Considering that all three epitaxial layers in each sample have the same Al content, this confirms the doping dependent etch selectivity of the electrochemical etching process. A similar etch selectivity has previously been reported for GaN.<sup>6</sup> The morphology of the sacrificial layer after the etching depends on the applied etching voltage. Complete etching was achieved for a sacrificial layer with an Al-content of 50% using an etching voltage of 30 V, as seen in the SEM image, which shows a continuous airgap and smooth etched surfaces. An etching voltage of 25 V yielded an almost completely removed sacrificial layer with few residues [see Fig. 3(b)]. Etching voltages of 20 V and 15 V, on the other hand, resulted in a porous sacrificial layer. Figures 3(c) and 3(d) show that the average pore diameter is larger at the higher voltage. The dependence of the etching type including the pore diameter on the applied etching voltage is similar to previous studies for GaN.<sup>10</sup> In addition to the morphology dependence on the etching voltage, also the influence of the Al content was investigated. Based on the morphology of the sacrificial layer after etching, all samples were categorized into complete etching of the sacrificial layer or porous etching. Figure 4 shows the dependence of the etching type on the Al content of the sacrificial layer and the applied etching voltage. The absolute values of the required bias voltage also include the different voltage drops at the contact and in the sample structure, which could not be quantified. The lateral etch rate was calculated based on optical microscopy images. It is on average around 40  $\mu\text{m}/\text{min}$  for all samples for which the sacrificial layer is completely etched, except samples with an Al content of 50% in the sacrificial layer for which the rate was around 18  $\mu\text{m}/\text{min}$ . The etch rate was lower in the samples where the sacrificial layer only got porosified with an etch rate below 10  $\mu\text{m}/\text{min}$ . The correlation of the aluminum content of the sacrificial layer and the required etching voltage is due to the working principle of electrochemical etching, which is based on the generation of holes ( $h^+$ ) at the AlGaIn/electrolyte interface. These holes oxidize AlGaIn at the interface, and the oxidized material can be dissolved by the electrolyte. Based on the oxidation states of Al and Ga<sup>17</sup> and previous works,<sup>12,18</sup> the following reaction equation is proposed:



**FIG. 3.** SEM cross-sectional images of four samples with a sacrificial layer containing 50% Al, which were etched at (a) 30 V, (b) 25 V, (c) 20 V, and (d) 15 V.

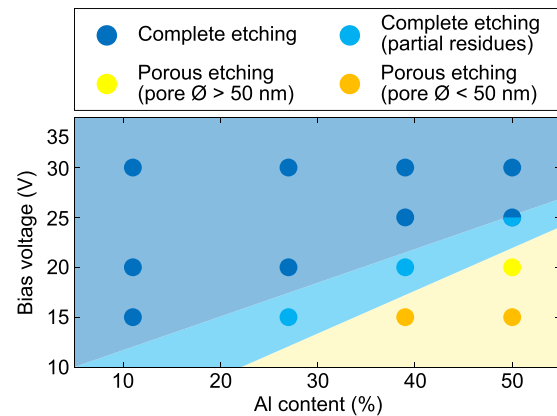


**FIG. 4.** Morphology of the sacrificial layer after the electrochemical etching as a function of bias voltage and aluminum content of the sacrificial layer.



The required holes ( $h^+$ ) are generated by Zener tunneling from the valence band to the conduction band and/or avalanche breakdown in the depletion region.<sup>18</sup> The influence of the Al content on the Fermi level is negligible due to a similar donor ionization energy.<sup>19</sup> Assuming a fixed redox level for the electrolyte, the built-in potential increases with the increasing Al content because the electron affinity decreases.<sup>20</sup> Accordingly, the depletion region width in the semiconductor increases with the increasing Al content. To achieve tunneling from the valence band to the conduction band, the applied bias voltage including the built-potential has to exceed the bandgap. Therefore, the required bias voltage for the tunneling depends on the valence band edge position, which is consequently larger for the higher Al content. Further, the required bias voltage is also influenced by additional factors such as surface states in the semiconductor, interface charges,<sup>7</sup> potential drop in the Helmholtz layer of the electrolyte, and geometrical factors in the setup, which reduce the conductivity of the electrolyte, which is beyond the scope of this work.

Fabricated membranes were investigated using atomic force microscopy (AFM) to obtain the topography of the etched surface and photoluminescence (PL) to measure the membranes' optical properties. The membranes were picked up using a thermal release tape on a Si carrier to access the etched N-polar side. Figure 5(a) shows the structure of the as-grown sample with 27% Al, and Fig. 5(d) shows an AFM scan of its top surface. The sample structure for the transferred membrane is illustrated in Fig. 5(b), an optical microscopy image of the transferred membrane is shown in Fig. 5(c), and an AFM image of the etched (N-polar) surface is shown in Fig. 5(e). Both AFM scans show the same macroscopic topography mainly dominated by large hillocks typical for AlGaIn growth.<sup>15</sup> Thus, the epitaxially defined morphology is conserved in the etching process. 1  $\mu\text{m} \times 1 \mu\text{m}$  AFM scan areas yield a root-mean square roughness of 3.5 nm after the electrochemical etching [see the inset of Fig. 5(e)].

To investigate that transferred devices are not affected by the electrochemical etching process, MQW structures were grown, underetched, transferred, and characterized. A 4  $\mu\text{m}$  thick relaxed silicon doped  $\text{Al}_{0.5}\text{Ga}_{0.5}\text{N}$  pseudosubstrate<sup>15,21</sup> with a Si concentration of  $2 \times 10^{18} \text{ cm}^{-3}$  was grown. This was followed by a 130 nm thick  $\text{Al}_{0.37}\text{Ga}_{0.63}\text{N}:\text{Si}$  sacrificial



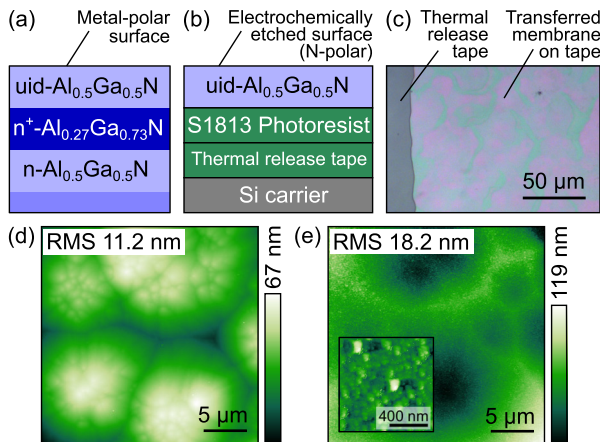


**FIG. 5.** (a) Structure of the as-grown epitaxial structure, (b) sample structure for the transferred membrane, (c) optical microscopy image of the transferred membrane, (d) AFM scan of the top surface (Ga-polar) of the as-grown epitaxial structure, and (e) AFM scan of the etched (N-polar) surface of the transferred membrane, with an inset of an AFM scan over an area of  $1 \mu\text{m} \times 1 \mu\text{m}$ .

layer with a Si-concentration of  $2 \times 10^{19} \text{ cm}^{-3}$ , embedded into a 500 nm thick  $\text{Al}_{0.5}\text{Ga}_{0.5}\text{N}$ :Si layer with a reduced Si-concentration of  $0.5 \times 10^{18} \text{ cm}^{-3}$ . The Al content in the sacrificial layer was chosen as low as 37% to maximize the contrast to the surrounding layer but high enough to be transparent for the emitted light for on-wafer testing. On top of that, a  $\text{Al}_{0.5}\text{Ga}_{0.5}\text{N}$ :Si current spreading layer for the MQW structure was grown. This was followed by a threefold  $\text{InAlGaN}$  MQW active region. The  $\text{InAlGaN}$  QWs with an Al-content of 21% and a thickness of 2 nm are separated by 5 nm thick barriers with an Al-content of 30%. Subsequently, an  $\text{Al}_{0.75}\text{Ga}_{0.25}\text{N}$  electron blocking layer and a Mg-doped  $\text{AlGaIn/AlGaIn}$  superlattice are grown. Finally, the structure was capped by a 20 nm thick  $\text{GaIn:Mg}$  contact layer [see Fig. 6(a)].<sup>15</sup> The epitaxial layers were patterned into circular mesas using ICP-RIE etching, and a Pd p-contact was deposited. The mesas were partially covered by a  $1 \mu\text{m}$  sputtered  $\text{SiO}_2$  layer to prevent parasitic electrochemical etching, and a Ti/Au (10/300 nm) bondpad was deposited on top. The mesas were underetched using electrochemical etching at a voltage of 25 V. Finally, the underetched MQW structures were transferred to a Si carrier with a Ti/Au (10/300 nm) bonding layer using thermocompression bonding at  $300^\circ\text{C}$  [see Fig. 6(b)].

To investigate the optical properties of the active region, room temperature PL measurements were performed using a Ti:sapphire laser with an emission wavelength of 275 nm and an average power of 1.2 mW (spot diameter of  $50 \mu\text{m}$ ) at a repetition rate of 80 MHz and a pulse duration of 140 fs. The PL spectrum for the as-grown and transferred MQW structures is shown in Fig. 6(c). The QW spectra for the as-grown and transferred MQW structures are presented normalized because of the different excitation conditions. A redshift in the peak wavelength is seen from 309 nm for the as-grown epitaxial structure to 311 nm for the transferred MQW structure. This shift of 2 nm could be caused by small local variations in the Al-composition and thickness over the sample, residual strain in the epitaxy, and process induced strain. To further quantify any potential process related degradation of the active region, the carrier lifetime for the as-grown MQW

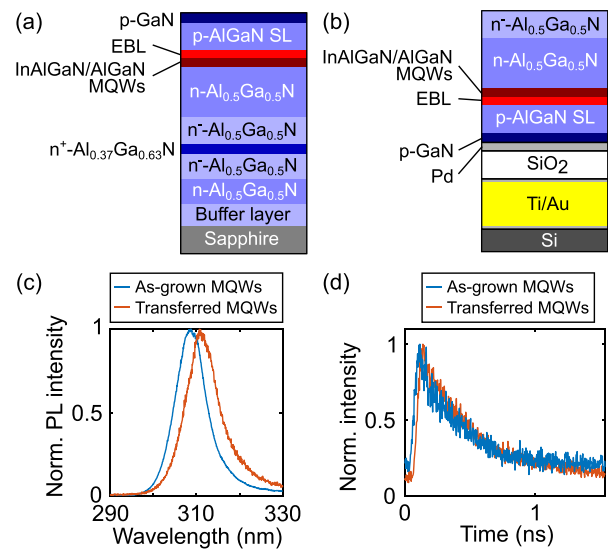


**FIG. 6.** (a) Sample structure of the as-grown MQW structure, (b) sample structure of the transferred MQW containing structure, (c) PL spectrum of the as-grown MQW structure probed from the Ga-polar side and the transferred MQW containing structure probed from the etched N-polar side, and (d) time-resolved PL of the same structures as in (c).

structure and the transferred MQW structure was compared by time-resolved PL measurements. Time-resolved PL excitation was performed in a similar manner to the time-integrated PL measurements. For detection, a spectrometer and a streak camera operating in the synchroscan mode were used. The excitation wavelength of 275 nm assured that carriers were generated mainly in the QW region. PL decay times in the QWs of the as-grown and lifted-off MQW structures were  $340 \pm 30$  ps and were not affected by the lift-off process. This confirms that the electrochemical etching and transfer process do not influence the quality of the QWs and, hence, are an appropriate process for fabrication of devices based on free-standing membranes.

In conclusion, we have demonstrated a method to laterally etch a sacrificial layer of  $\text{AlGaIn}$  and thereby separate a device layer stack from the substrate with a well-defined thickness and smooth etched surface. We have shown complete removal of an  $\text{AlGaIn}$ -layer with an Al-content of up to 50% using electrochemical etching. The required bias voltage to achieve complete etching increases with the increasing Al-composition in the sacrificial layer. Etched surfaces show an RMS roughness of the N-polar  $\text{AlGaIn}$  surface of 3.5 nm for  $1 \mu\text{m} \times 1 \mu\text{m}$  scan areas. Time-resolved PL measurements at room temperature showed no degradation of the optical quality of the QWs in electrochemically underetched and transferred MQW structures. Thus, this method offers a way for the realization of thin-film devices with high-quality epitaxial  $\text{AlGaIn}$  layers.

The project was financially supported by the Swedish Foundation for Strategic Research, the Swedish Energy Agency, the Swedish Research Council (Project Nos. 2016-04686 and 2018-00295), the German Federal Ministry of Education and Research (BMBF) within the “Advanced UV for Life” project, and the

Deutsche Forschungsgemeinschaft (DFG) within the Collaborative Research Center “Semiconductor Nanophotonics” (SFB 787).

## REFERENCES

- <sup>1</sup>*III-Nitride Ultraviolet Emitters*, Springer Series in Materials Science Vol. 227, edited by M. Kneissl and J. Rass (Springer International Publishing, 2016).
- <sup>2</sup>H. Amano, Y. Baines, E. Beam, M. Borga, T. Bouchet, P. R. Chalker, M. Charles, K. J. Chen, N. Chowdhury, R. Chu, C. D. Santi, M. M. D. Souza, S. Decoutere, L. D. Cioccio, B. Eckardt, T. Egawa, P. Fay, J. J. Freedman, L. Guido, O. Hberlen, G. Haynes, T. Heckel, D. Hemakumara, P. Houston, J. Hu, M. Hua, Q. Huang, A. Huang, S. Jiang, H. Kawai, D. Kinzer, M. Kuball, A. Kumar, K. B. Lee, X. Li, D. Marcon, M. Mrz, R. McCarthy, G. Meneghesso, M. Meneghini, E. Morvan, A. Nakajima, E. M. S. Narayanan, S. Oliver, T. Palacios, D. Piedra, M. Plissonnier, R. Reddy, M. Sun, I. Thayne, A. Torres, N. Trivellin, V. Unni, M. J. Uren, M. V. Hove, D. J. Wallis, J. Wang, J. Xie, S. Yagi, S. Yang, C. Youtsey, R. Yu, E. Zanon, S. Zeltner, and Y. Zhang, “The 2018 GaN power electronics roadmap,” *J. Phys. D* **51**, 163001 (2018).
- <sup>3</sup>M. K. Kelly, O. Ambacher, R. Dimitrov, R. Handschuh, and M. Stutzmann, “Optical process for liftoff of group III-nitride films,” *Phys. Status Solidi A* **159**, R3–R4 (1997).
- <sup>4</sup>H. K. Cho, O. Krüger, A. Külberg, J. Rass, U. Zeimer, T. Kolbe, A. Knauer, S. Einfeldt, M. Weyers, and M. Kneissl, “Chip design for thin-film deep ultraviolet LEDs fabricated by laser lift-off of the sapphire substrate,” *Semicond. Sci. Technol.* **32**, 12LT01 (2017).
- <sup>5</sup>H. Yoshida, Y. Takagi, M. Kuwabara, H. Amano, and H. Kan, “Entirely crack-free ultraviolet GaN/AlGaIn laser diodes grown on 2-in. sapphire substrate,” *Jpn. J. Appl. Phys., Part 1* **46**, 5782–5784 (2007).
- <sup>6</sup>J. Park, K. M. Song, S.-R. Jeon, J. H. Baek, and S.-W. Ryu, “Doping selective lateral electrochemical etching of GaN for chemical lift-off,” *Appl. Phys. Lett.* **94**, 221907 (2009).
- <sup>7</sup>T.-H. Chang, K. Xiong, S. H. Park, G. Yuan, Z. Ma, and J. Han, “Strain balanced AlGaIn/GaN/AlGaIn nanomembrane HEMTs,” *Sci. Rep.* **7**, 6360 (2017).
- <sup>8</sup>A. W. Bruch, K. Xiong, H. Jung, X. Guo, C. Zhang, J. Han, and H. X. Tang, “Electrochemically sliced low loss AlGaIn optical microresonators,” *Appl. Phys. Lett.* **110**, 021111 (2017).
- <sup>9</sup>J.-H. Kang, D. K. Jeong, and S.-W. Ryu, “Transparent, flexible piezoelectric nanogenerator based on GaN membrane using electrochemical lift-off,” *ACS Appl. Mater. Interfaces* **9**, 10637–10642 (2017).
- <sup>10</sup>D. Chen, H. Xiao, and J. Han, “Nanopores in GaN by electrochemical anodization in hydrofluoric acid: Formation and mechanism,” *J. Appl. Phys.* **112**, 064303 (2012).
- <sup>11</sup>P. Griffin, T. Zhu, and R. Oliver, “Porous AlGaIn-based ultraviolet distributed Bragg reflectors,” *Materials* **11**, 1487 (2018).
- <sup>12</sup>L. Zhang, J. Yan, Q. Wu, Y. Guo, C. Yang, T. Wei, Z. Liu, G. Yuan, X. Wei, L. Zhao, Y. Zhang, J. Li, and J. Wang, “Improved crystalline quality of Al-rich n-AlGaIn by regrowth on nanoporous template fabricated by electrochemical etching,” *J. Nanophotonics* **12**, 043509 (2018).
- <sup>13</sup>G.-J. Wang, B.-S. Hong, Y.-Y. Chen, Z.-J. Yang, T.-L. Tsai, Y.-S. Lin, and C.-F. Lin, “GaN/AlGaIn ultraviolet light-emitting diode with an embedded porous-AlGaIn distributed Bragg reflector,” *Appl. Phys. Express* **10**, 122102 (2017).
- <sup>14</sup>F.-H. Fan, Z.-Y. Syu, C.-J. Wu, Z.-J. Yang, B.-S. Huang, G.-J. Wang, Y.-S. Lin, H. Chen, C. H. Kao, and C.-F. Lin, “Ultraviolet GaN light-emitting diodes with porous-AlGaIn reflectors,” *Sci. Rep.* **7**, 4968 (2017).
- <sup>15</sup>J. Enslin, F. Mehnke, A. Mogilatenko, K. Bellmann, M. Guttman, C. Kuhn, J. Rass, N. Lobo-Ploch, T. Wernicke, M. Weyers, and M. Kneissl, “Metamorphic Al<sub>0.5</sub>Ga<sub>0.5</sub>N:Si on AlN/sapphire for the growth of UVB LEDs,” *J. Cryst. Growth* **464**, 185–189 (2017).
- <sup>16</sup>C. Zhang, G. Yuan, A. Bruch, K. Xiong, H. X. Tang, and J. Han, “Toward quantitative electrochemical nanomachining of III-nitrides,” *J. Electrochem. Soc.* **165**, E513–E520 (2018).
- <sup>17</sup>M. Pourbaix, *Atlas of Electrochemical Equilibria in Aqueous Solutions* (National Association of Corrosion Engineers, 1974), Chap. 4.
- <sup>18</sup>W. J. Tseng, D. H. van Dorp, R. R. Lieten, P. M. Vereecken, and G. Borghs, “Anodic etching of n-GaN epilayer into porous GaN and its photoelectrochemical properties,” *J. Phys. Chem. C* **118**, 29492–29498 (2014).
- <sup>19</sup>R. Collazo, S. Mita, J. Xie, A. Rice, J. Tweedie, R. Dalmau, and Z. Sitar, “Progress on n-type doping of AlGaIn alloys on AlN single crystal substrates for UV optoelectronic applications,” *Phys. Status Solidi C* **8**, 2031–2033 (2011).
- <sup>20</sup>S. P. Grabowski, M. Schneider, H. Nienhaus, W. Mnch, R. Dimitrov, O. Ambacher, and M. Stutzmann, “Electron affinity of Al<sub>x</sub>Ga<sub>1-x</sub>N(0001) surfaces,” *Appl. Phys. Lett.* **78**, 2503–2505 (2001).
- <sup>21</sup>A. Mogilatenko, J. Enslin, A. Knauer, F. Mehnke, K. Bellmann, T. Wernicke, M. Weyers, and M. Kneissl, “V-pit to truncated pyramid transition in AlGaIn-based heterostructures,” *Semicond. Sci. Technol.* **30**, 114010 (2015).